Materials Physics and Mechanics. 2022;48(3): 342-354
Research article
http://dx.doi.org/10.18149/MPM.4832022_5

Submitted: January 26, 2022
Approved: April 22, 2022
Accepted: April 25, 2022

Comparison of mechanical strain measurement accuracy of fiber-optic sensor and smart-layer

G.S. Shipunov, M.A. Baranov✉, A.S. Nikiforov, F.R. Khabibrakhmanova

Perm National Research Polytechnic University, 29 Komsomolsky Ave., Perm, Russia, 614990

✉ maximbaranov.123@gmail.com

Abstract. Due to its fragility, fiber optic sensor (FOS) embedded into constructions made of carbon fiber reinforced polymer, can be broken both while it is manufacturing at the point of embedding into construction, and during its operation. This can lead to the inability to further monitoring of the construction strains. Usage of a specific thin Smart-layer for protection of FOS is proposed by the authors. For the Smart-layer manufacturing, 3D printing technology was used. The spectra of fiber Bragg grating (FBG) before and after layer printing have been analyzed, remaining compression strains were recorded. A mechanical test of a sample with surface-mounted FOS along with a Smart-layer was performed in order to measure the precision of strain detection by the Smart-layer. Some inaccuracy in strain detection was found during the analysis of the results. In order to find out the error in strain measured by a Smart-layer, a mechanical test of a full-sized bulkhead in a complex stress-strain state was performed

Keywords: fiber optic sensor, structural health monitoring, fused deposition method, Smart-layer, carbon fiber reinforced polymer

Acknowledgements*. The results were obtained during the fulfillment of the state task of the Ministry of Science and Higher Education of the Russian Federation for the implementation of fundamental scientific research (project No. FSNM-2020-0026).*

Citation: Shipunov GS, Baranov MA, Nikiforov AS, Khabibrakhmanova FR. Comparison of mechanical strain measurement accuracy of fiber-optic sensor and smart-layer. *Materials Physics and Mechanics*. 2022;48(3): 342-354. DOI: 10.18149/MPM.4832022_5.

1. Introduction

Nowadays, the safety and reliability of structures used in civilian, space, and aviation branches, are of principal concern. In order to meet these requirements, periodic non-destructive examinations are usually performed. However, such periodic examinations cannot totally ensure the integrity of a structure and guarantee the safety of its usage [1-3]. This was the reason for scientists to start research on so-called "Structural health monitoring systems" (SHM) based on different kinds of sensors (strain gauges or fiber optic sensors (FOS)), mounted at / embedded into the structure if it is possible.

Monitoring systems based on FOS are widely used in the aviation industry [4]. For example, some experimental investigations of FOS embedded into composite parts of helicopters, are presented and summarized in the article [5]. The problem of embedding optical fiber into carbon fiber reinforced polymer (CFRP) has been considered by the authors; the data provided by FOS embedded into a helicopter longeron prone to exfoliation caused by

dynamic stress has been published. Monitoring of cracks in helicopter hulls caused by metal fatigue with the help of a fiber Bragg grating-based FOS network has been described in the article [6]. Practical usage of FOS for structural monitoring of propeller aircraft and sailing yacht parts has been considered in the article [7]. FOS were embedded into a 35-meter carbon mast of a yacht and mounted at the surface of Jetstream airplane wing. Data from the sensors of the airplane were obtained in real-time while flying in extreme conditions. Another case, when sensors were embedded into airplane wings, is described in the article [8]. Bragg grating-based FOS were used for real-time measurement of dynamic strains during wing testing in a wind tunnel. Readings from the FOS were compared with those from strain gauges and piezoelectric sensors. Good convergence of all the systems has been observed during bench testing. The process of embedding 20 FOS into a longeron of UAV was described in the article [9]. The authors covered the process of development and building of FOS data transmission system mounted at UAV, and described the flight tests when data from FOS were transmitted to the ground-based receiver and deciphered.

Thus, FOS-based monitoring systems are essential for monitoring different kinds of structures. However, most authors mention some difficulties when mounting FOS at the surface or embedding them into a structure. Particularly, they note the fragility of optical fiber, the complexity of accurate sensor positioning, and ensuring the integrity of FOS emerging from a CFRP construction [10-12].

For solving the problems mentioned, the authors use different kinds of "wrappings" for FOS protection. Acellent Technologies, Inc. developed a Smart-layer that allows protection of various types of sensors (FOS, piezoelectric) and their outputs to ensure the accuracy of the sensing element in the monitored environment [13]. In[14], the company mentioned described their own technology for creating the Smart-layer, consisting of a network of piezoelectric sensors that were placed between a polyimide film and coated with epoxy resin. This technology ensures the integrity of the sensors. It can be used for surface monitoring of structures, but it cannot be used for embedding sensors directly into CFRP structures since polyimide films have poor adhesion to carbon fiber reinforced polymers. The thickness of such a layer can be up to 2-4 mm, so it can significantly affect the physical and mechanical characteristics of such structures.

Yoon H.J. et al. used Brillouin backscattering-based FOS for analysis of longitudinal strains of a 40.26-meter long railway bridge when a train had been moving on it at a speed of 15 kilometers per hour [15]. FOS were wrapped into Hytrel thermoplastic elastomer buffer, additionally protected with 0.3 mm thick polyethylene film, and mounted on a rail. The values of longitudinal strains obtained from FOS were compared to the results from strain gauges.

The authors of the article [16] used two fiber Bragg gratings wrapped into a 250 mm length glass tube for diagnosing the stress-strain state of a bridge. The glass tube was fixed to the concrete surface of the bridge with bolts. The authors note that such glass tube containing FOS allows obtaining a full picture of the stress-strain state, however, the cost of such tubes is rather high. Therefore, in their work [17] the authors explored the possibility of manufacturing simple and inexpensive wrapping for FOS capable of providing high quality and reproducibility of strain measurement. While developing such kind of wrapping, the authors defined the following requirements: it should be suitable both for surface mounting (i. e., withstand harsh environmental conditions) and direct embedding into concrete. The authors used photopolymeric resin 3D printing technology. At first, U-shaped substrate was made, and optical fiber was placed inside. Afterward, the substrate was filled with Duralco glue. The thickness of such a package reached 5 mm. The authors conducted some mechanical tests of the concrete beams with sensor packages mounted. After having obtained the test results, they decided to modify the design of the package. The authors then printed U-shaped substrate and cover plate separately. Optical fiber was placed on U-shaped substrate,

covered with glue, and protected by a plate. The thickness of the resulting package was comparable to that of the first version. However, the authors note that FOS sensitivity has decreased. Hence, the authors compared the results of concrete beam mechanical testing with different types of sensor packages. They note that both types are suitable for surface mounting and embedding into constructions; the second design is more advanced and durable, but less sensitive than the first one.

The analysis of the articles mentioned can lead to the conclusion that nowadays FOS packages are manufactured mainly by the technology of gluing together polyamide film layers, and by using additive technologies. This is due to the fact that additive methods are gaining in popularity over the past decades. 3D manufacturing methods such as fused deposition method (FDM) and stereolithography (SLA) are the most common thanks to the possibility of rapid prototyping, low cost of the final part, and the use of various engineering plastics with the required characteristics [18].

Thus, different types of FOS wrappings can provide protection for sensors. However, the majority of packages were designed for surface monitoring of different types of constructions (bridges, rails, pipes) or embedding into concrete, so their dimensions are quite large, and their thickness is up to 3-5 mm. They are not suitable for embedding into CFRP, since such a process can significantly change the physical and mechanical properties of CFRP structures. Hence, the development of thin Smart-layers is a relevant task nowadays.

Several prototypes of Smart-layers have been developed and manufactured at the Research and Educational Center of Aviation Composite Technologies at Perm National Research Polytechnic University. They were embedded into sample constructions made of CFRP and tested. It has been discovered that the embedding process has a negligible effect on the physical and mechanical characteristics of the structures. However, the correctness of strain measurement by the Smart-layers is still the issue of further research. Thus, the aim of this paper is to investigate the effect of the wrapping on the measurement accuracy of FOS.

2. Smart-layer manufacturing

Since Smart-layer is intended to be used both at the surface and inside CFRP, it is necessary to consider the temperature used for manufacturing CFRP samples and constructions. Usually, it is 130-180°C, so the melting point of materials used for building Smart-layers has to be higher than this.

Considering the condition mentioned, it was decided to use the nylon filament (ePA from eSUN) which is printed at 230-260°C and therefore meets the requirements.

Smart-layers were manufactured on a CreatBot F430 FDM 3D printer, which has the following characteristics: bed heat temperature of 120°C, max nozzle heat temperature of 420°C, and hot-chamber device with a constant temperature of 70°C. This 3D printer is a part of the unique research facility "Research complex for scientific and technological research in the field of creating products made of polymer composite materials".

Smart-layer manufacturing consisted of two stages. At the first stage, the lower half of the layer containing a rectangular-shaped groove with dimensions of 0.2×0.16 millimeters was printed, as shown in Fig. 1a. For ensuring the precise placement of the optical fiber inside Smart-layer, the fiber was stretched, loaded into the groove, and had both its ends fixed with sticky tape to the printer bed.

In the second stage, the printing program was resumed and the upper half of the Smart-layer was printed. Fig. 1b represents Smart-layer's second half print scheme. The optical fiber containing fiber Bragg grating (FBG) for a Smart-layer was manufactured by "Inversia Sensor" company. The fiber had a 0.02 mm thick polyamide covering, thus its operating temperature range is from -200°C to 350°C. The FBG length was 5 mm, its resonant wavelength was 1528.17 nm, the reflection coefficient was 70.49%, the spectrum peak

width was 0.155 nm, suppression of side peaks was 9.6 dB. The diameter of the optical fiber was 0.156 mm.

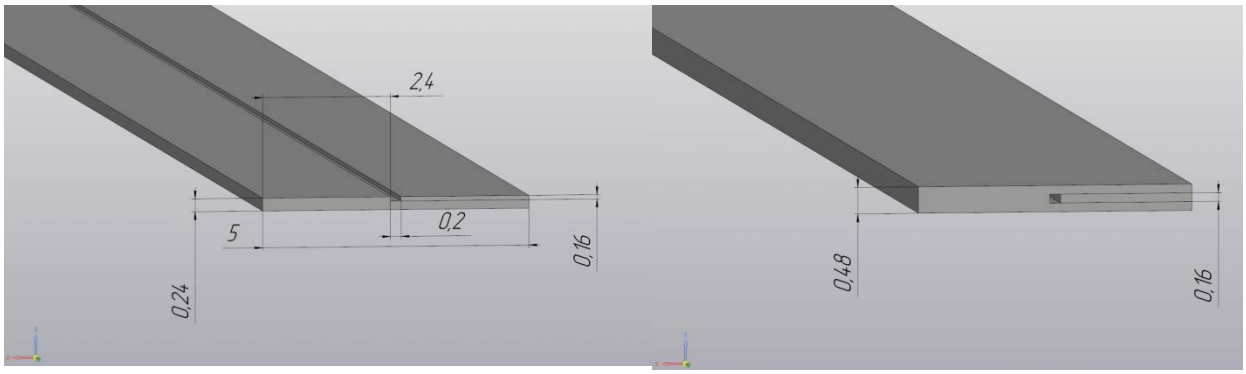

(a) (b)

Fig. 1. Smart-layer manufacturing scheme: Smart-layer's first half print scheme (a); Smart-layer's second half print scheme (b)

Printing was performed with the following parameters: the substrate temperature was 120°C, printing temperature was 270°C, printing speed was 60 mm/s. It is necessary to mention that optical fiber was rigidly fixed inside the Smart-layer (without any slippery) due to the shrinking of the plastic used. The manufactured layer is presented in Fig. 2. After completion of the printing process, it was connected to a laser source for testing. As it is shown in Fig. 2, optical fiber remained intact and was still capable of transmitting the light.

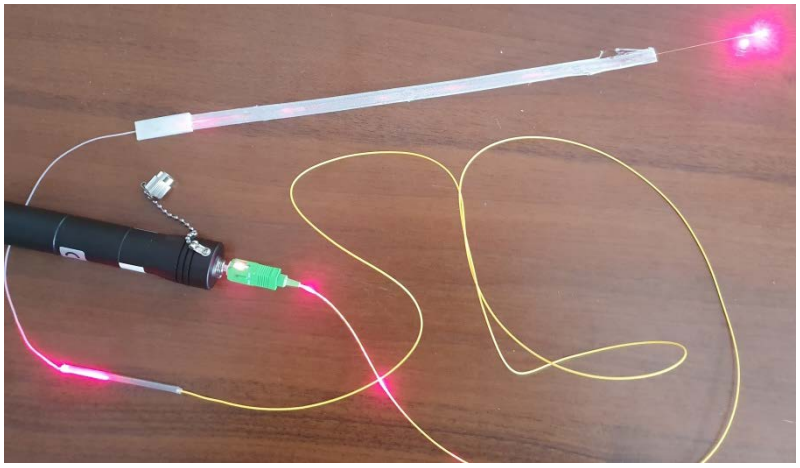

Fig. 2. Smart-layer manufactured of nylon by using FDM printing technology

It is known that plastic shrinks after printing because of cooling, so fiber Bragg grating in the Smart-layer is expected to have some residual compression strains. For investigating the impact of residual strains on a spectrum of fiber Bragg grating, the corresponding spectra were studied before and after printing. They are presented in Fig. 3.

The shift of the spectrum peak in the sealed FBG compared to the one of the original FBG allows determining the shift of the resonant wavelength of the signal reflected from the sensor which is caused by the combined impact of mechanical strain and temperature. Analysis of the spectrum obtained revealed a 2.175 nm change in resonant wavelength. More detailed analysis showed that FBG sealing didn’t result in peak split; therefore, the double refraction effect did not happen. Double refraction can be caused by temperature strains and material shrinking in the process of manufacturing [19]. Double refraction usually leads to profile strain and some changes in the shape of the peak, which, in turn, lowers measurement

precision and results in doubling the reflection spectrum, which complicates determining the value measured. The next stage of the research is aimed at comparing strains registered during mechanical tests by FOS and Smart-layer.

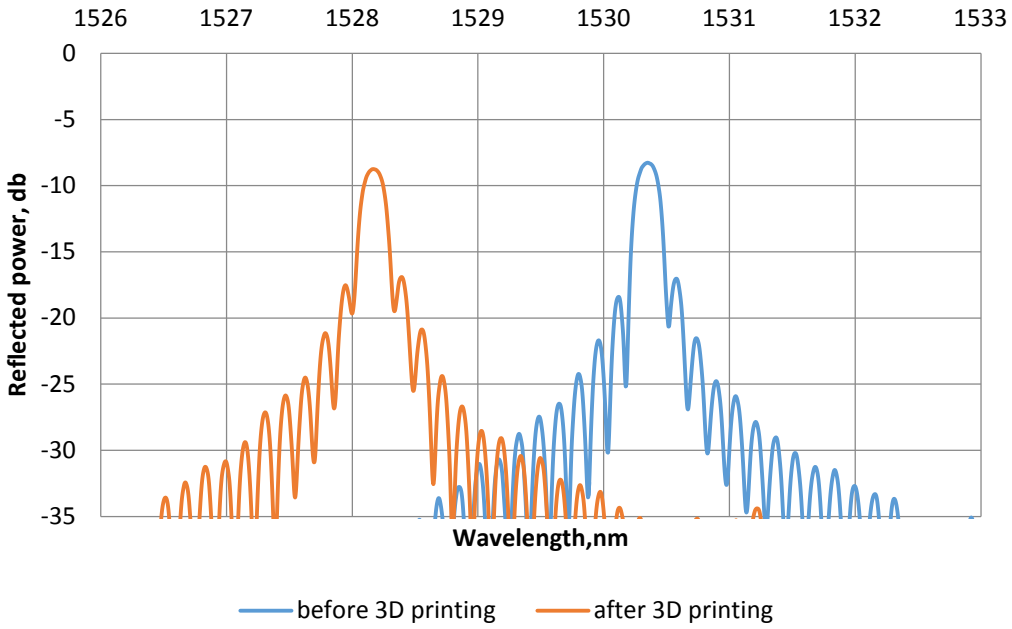

Fig. 3. Distribution of reflected signal wavelength before and after 3D printing

3. Comparison of fiber-optic sensor and Smart-layer measurements of strain under single-axis load

For detecting possible errors in registering strains by Smart-layer, a CFRP plate with reinforcement scheme $[0,45]_5$ was made. It was cut into six 310×22.5×2.3 mm samples. Five of them were used for determining the critical load that breaks the sample when applied. Finding out the critical load value is necessary to avoid the destruction of control sample with FOS and Smart-layer.

Statistical processing of experimental data was performed according to the following set of correlations (1):

$$\begin{cases} \overline{x} = \dfrac{1}{n}\sum_{i=1}^{n} x_i, \\ s = \sqrt{\dfrac{1}{n-1}\sum_{i=1}^{n}\left(x_i - \overline{x}\right)^2}, \\ v = \dfrac{s}{\overline{x}} \cdot 100\,(\%), \end{cases} \tag{1}$$

where $\overline{x}$ is the mean value; s is standard deviation of a value; v is coefficient of variation.

The results of statistical processing of all the data obtained as the result of mechanical tests of the samples are presented in Table 1.

According to the mechanical stretching tests of the five samples, the mean value of critical load was 34.85 kN. The load on the control sample was limited up to 15% of the critical value stated above. Optical fiber and Smart-layer were mounted in such a way that every grating was equally distant from the symmetrical center of the tested sample. The fiber and the Smart-layer were fixed with epoxy resin. The arrangement of FOS and Smart-layer at

the CFRP sample is schematically presented in Fig. 4a. The photo of the sample secured in the testing unit is presented in Fig. 4b.

Table 1. Statistical Processing of Mechanical Test Results

$n=5$	σ_{max}, MPa	F_{max}, kN	h, mm	w, mm
$\overline{x}$	665.45	34.85	2.32	22.7
s	26.68	0.46	0.06	0.06
$v,\%$	4	1.32	2.75	0.28

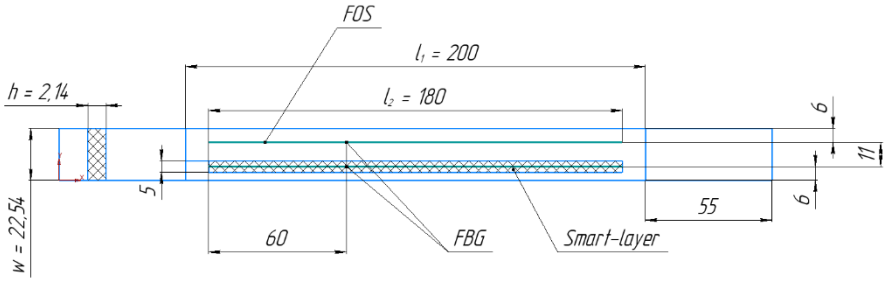

(a)

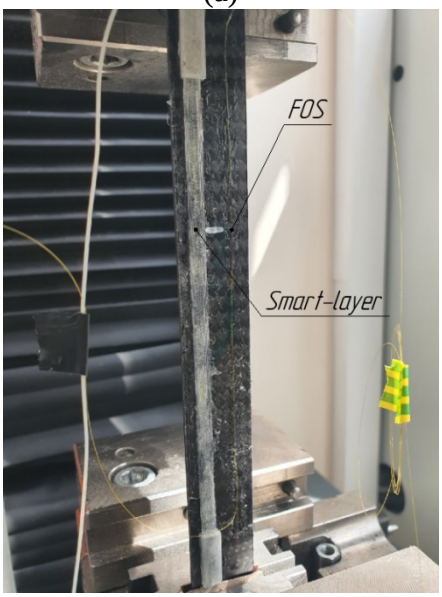

(b)

Fig. 4. The arrangement of FOS and Smart-layer. *(a)* FOS placement scheme; *(b)* control sample with FOS and Smart-layer secured in the testing unit

During mechanical tests of the control sample, a special construction monitoring system was used. It was developed by our research team and consists of a monitored object with mounted Smart-layer and FOS; the interrogator device that is necessary for data exchange with FOS in the Smart-layer; special software that initiates data transfer between the optical fiber and the interrogator, and subsequently processes the data received [20].

The interrogator is a device measuring wavelengths of the light reflected from the fiber Bragg gratings. It operates by measuring the power of the light beam at the output of periodically rearranged selective optical filter in the measured range of wavelengths. The interrogator creates a ray of light directed at sensor (Bragg grating). The reflected signal is

processed by the interrogator and is transferred to the computer. The information received from FOS is presented with the help of specialized software.

The resonant wavelength of Bragg grating λ_β depends on the effective refractive index and the grating period. It is expressed by the following correlation [21]:

$$\lambda_\beta = 2n\Lambda, \tag{2}$$

where n is effective refractive index, Λ is period of fiber Bragg grating. The shift of the spectrum position is defined by the following correlation:

$$\Delta\lambda_\beta = 2\left(\Lambda\frac{\partial n}{\partial l} + n\frac{\partial \Lambda}{\partial l}\right)\Delta l + 2\left(\Lambda\frac{\partial n}{\partial T} + n\frac{\partial \Lambda}{\partial T}\right)\Delta T. \tag{3}$$

The first summand of equation (3) is the impact of strain on the optic fiber. Its physical meaning lies in the change in grating period and refractive index, caused by the optical elasticity effect. The second summand represents the temperature impact on Bragg grating. The Bragg wavelength shift is caused by thermal expansion of quartz that leads to a change in the grating period and refractive index. According to [22], equation (3) can be presented as the following:

$$\Delta\lambda_\beta = \lambda_\beta\left(1 - p_e\right)\varepsilon + \lambda_\beta\left(\alpha + \xi\right)\Delta T, \tag{4}$$

where p_e is effective optical elasticity constant, α is linear thermal expansion coefficient, ξ is thermo-optic coefficient, ε is strain.

As the testing was conducted in normal conditions, there were no temperature changes during the experiment. Therefore, the second summand of the equation (4) can be neglected, so the equation (4) takes the following form:

$$\Delta\lambda_\beta = \lambda_\beta\left(1 - p_e\right)\varepsilon. \tag{5}$$

The effective optical elasticity coefficient is defined by the following:

$$p_e = \frac{n^2}{2}\left(p_{12} - \nu(p_{11} + p_{12})\right), \tag{6}$$

where p_{11}, p_{12} are Pockels coefficients of elastic-optical tensor.

Substituting the values of Pockels coefficients (p_{11}=0.113, p_{12}=0.252, ν=0.16, n=1.4682) into the equation (4) and excluding temperature strains, we get the formula for strain calculation for any given time:

$$\varepsilon = \frac{1}{0.78}\frac{\Delta\lambda_\beta}{\lambda_\beta}. \tag{7}$$

During the mechanical tests, dependencies of strains (registered by FOS and Smart-layer) upon time have been obtained. They are presented in Fig. 5.

During the test, when 5 kN load was applied to the sample, the strain registered by the fiber optic sensor was $\varepsilon = 0.099\%$, and the one registered by Smart-layer was $\varepsilon = 0.1\%$.

It should be noted that the accuracy of strain measurement by FOS is not considered in this work since the error of such measurements described in prior research works, does not exceed 6% [23]. The aim of this work is to identify the difference in strain values obtained from Smart-layer and FOS. The analysis of the data obtained leads to the conclusion that the error in strain values measured by Smart-layer is 8.23%. Thus, this error has to be taken into account when Smart-layers are used, and the monitoring system has to be calibrated considering the error of strain measurement.

It is known that full-scale constructions can be in a complex stress-strain state, so the error of strain measurement by Smart-layer on such constructions is to be found.

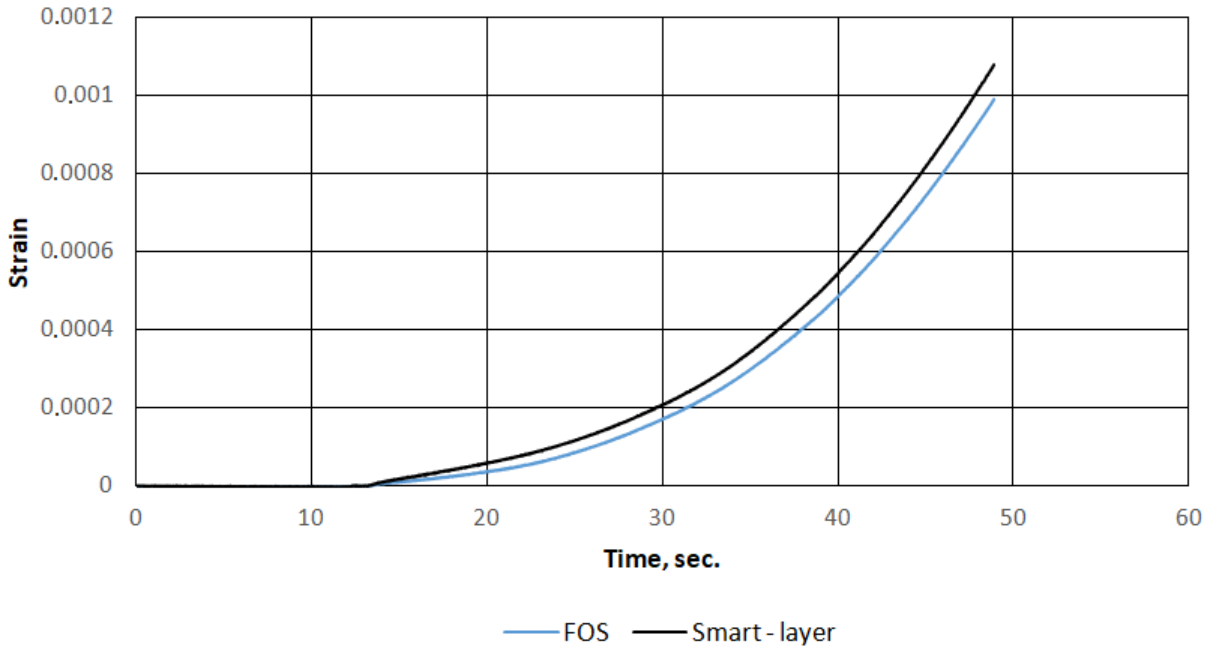

Fig. 5. Dependencies of strain value (registered by FOS and Smart-layer) upon time

4. Comparison of fiber-optic sensor and Smart-layer measurements of strain in combined stress-strain state of a bulkhead

The next stage of research is finding out the accuracy of strain measurement by Smart-layer which is mounted on a full-scale construction along with FOS. A CFRP bulkhead was chosen as the construction for the tests. A CFRP bulkhead is a U-shaped ring. The bulkhead is made of textile carbon fiber reinforced plastic with epoxy resin using resin transfer molding (RTM). The bulkhead consists of a solid circular U-shaped body and two flanges having some technological notches and mounting holes. The necessity of this experiment arises from possible confirmation of precise registration of strains in structure experiencing a complex (combined) stress-strain state.

For conducting mechanical tests, the bulkhead was secured on vertical supports. FOS and Smart-layer were mounted on a 740-mm long bulkhead segment. Static load was applied in the middle of the segment. FOS and Smart-layer were mounted at an equal 60 mm distance from the sector symmetry center. The sensor mounting scheme is presented in Fig. 6. Static load was also applied to the symmetry center of the bulkhead sector. A graduated load scheme was used in the experiment. It included 5 stages of load application. At the first stage of the experiment, a 150 N weight was placed on the platform attached to the bulkhead with a stud. At subsequent stages, the same weight was added until the load reached 750 N.

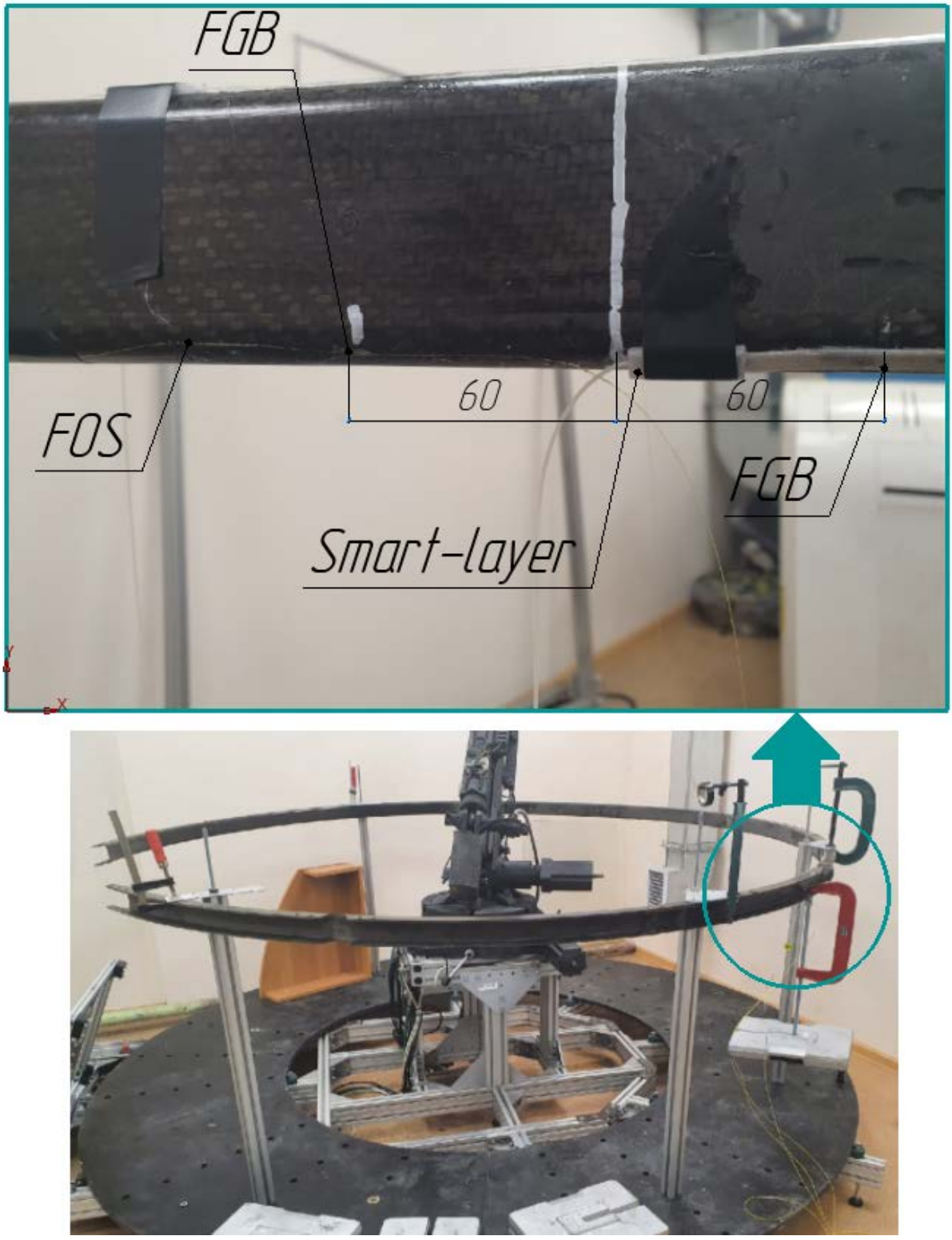

Fig.6. Mechanical test of the bulkhead. FOS placement scheme and application of load to the bulkhead segment center

During mechanical tests, for each stage of load application, the values of strain measured by Smart-layer and FOS, were obtained. They are presented in Fig. 7.

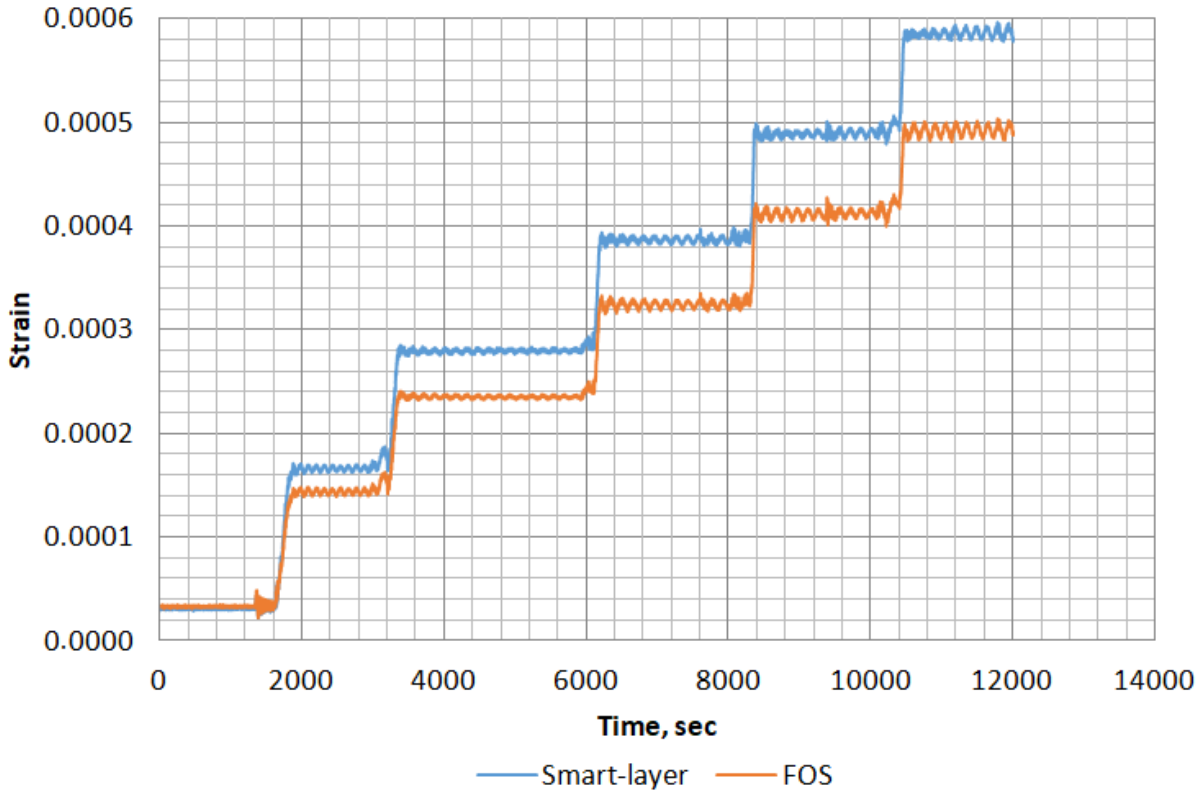

Fig. 7. Dependence of strain value (registered by FOS and Smart-layer) upon time during the process of graduated load application

For every pair of strain values (registered by FOS and Smart-layer), their difference and percentage deviation were calculated. Under 150 N load, strain registered by Smart-layer and FOS was 0.017% and 0.015% correspondingly. The difference between readings was 0.002%, and percentage deviation was 11.76%. At the next stage, the load applied to the bulkhead, was doubled. The difference between readings, in this case, was 0.004%, and percentage deviation was 14.29%. At the following three stages, the load was increased by 150 N every time. The difference between readings was 0.005%, 0.007%, 0.008% correspondingly. The percentage deviation was 13.16%, 14.29%, and 13.79% correspondingly. The measurement results obtained during the mechanical test are presented in Table 2.

Table 2. Strains Registered by FOS and Smart-layer During Graduated Load Application

F, N	$\varepsilon_{Smart-layer}, \%$	$\varepsilon_{FOS}, \%$	$\Delta\varepsilon, \%$	Percentage deviation, %
150	0.017	0.015	0.002	11.76
300	0.028	0.024	0.004	14.29
450	0.038	0.033	0.005	13.16
600	0.049	0.042	0.007	14.29
750	0.058	0.05	0.008	13.79

On the basis of the results obtained it can be concluded that the maximal difference between sensor readings was 14.29% (under 300 N and 600 N load), and minimal difference was 11.76% (under 150 N load). It should be noted that the difference between FOS and

Smart-layer readings has demonstrated continuous, almost linear growth as the load increased. However, there has not been found any obvious correlation between load value and percentage deviation. Hence, it can be supposed that in the case of further load increase, measurement error of Smart-layer compared to FOS will remain within 11.76% – 14.29% range.

5. Summary and Conclusion

Thus, within the research presented in the article, a Smart-layer has been manufactured using 3D printing technology. Spectra of the light waves reflected from Bragg grating before and after the printing have been analyzed. Some residual strains in the layer have been found, as indicated by a shift of resonant wavelength. Based on the shapes of spectra peaks, it can be stated that the double refraction effect doesn't appear when sealing FBG.

The mechanical test on stretching the sample with mounted FOS and Smart-layer has been carried out. The dependence of strain upon time under quasi-static single-axis load was obtained and analyzed; the measurement error of Smart-layer has been found to be 8.23%.

In order to find out the dependence of Smart-layer and FOS response deviation upon load in case of the complex stress-strain state, a mechanical test of a CFRP bulkhead has been carried out. A graduated 5-staged load was used in the experiment. For every stage, the values of the registered strains, the difference between sensor readings, and the percent deviation of the values have been recorded. During the analysis of the results obtained, it has been found that the difference of registered values of strain lies in a range from 11.76% to 14.29%, and the average difference is 13.46%.

As the result of mechanical tests, error of strain measurement by Smart-layer has been found out both for single-axis quasi-static and complex load; calibration coefficient that allows registering strain more precisely has been calculated. On the basis of the results obtained, the following conclusion can be drawn: the use of the proposed Smart-layer instead of FOS has been proved to be more innovative and efficient, due to time saving during FOS mounting. Moreover, it excludes the possibility of their damage during their mounting and dismantling.

The next stage of the research is to embed the FOS and Smart-layer into a sample and determine the error of strain measurement during mechanical tests, as well as carrying out mechanical tests of full-sized constructions made of CFRP and fitted with FOS and Smart-layer.

References

1. Yu F, Okabe Y. Linear damage localization in CFRP laminates using one single fiber-optic Bragg grating acoustic emission sensor. *Compos. Struct.* 2020;238: 1-10.
2. Tserpes KI, Karachalios V, Giannopoulos I, Prentzias V, Ruzek R. Strain and damage monitoring in CFRP fuselage panels using fiber Bragg grating sensors. Part I: Design, manufacturing and impact testing. *Compos. Struct.* 2014;107: 726-736.
3. Han T, Wu G, Lu Y. Crack monitoring using short-gauged Brillouin fiber optic sensor. *Measurement.* 2021;179: 1-13.
4. Di Sante R. Fibre optic sensors for structural health monitoring of aircraft composite structures: Recent advances and applications. *Sensors.* 2015;15(8): 18666-18713.
5. Ghoshal A, Ayers J, Gurvich M, Urban M, Bordick N. Experimental investigations in embedded sensing of composite components in aerospace vehicles. *Compos. Part B Eng.* 2015;71: 52-62.
6. Sbarufatti C, Manes A and Giglio M. Application of sensor technologies for local and distributed structural health monitoring. *Struct. Control Health Monit.* 2013;21(7): 1057-1083.

7. Read IJ, Foote PD. Sea and flight trials of optical fibre Bragg grating strain sensing systems. *Smart Mater. Struct.* 2001;10(5): 1085-1094.
8. Lee JR, Ryu CY, Koo BY, Kang SG, Hong CS, Kim CG. In-flight health monitoring of a subscale wing using a fiber Bragg grating sensor system. *Smart Mater. Struct.* 2003;12(1): 147-155.
9. Alvarez-Montoya J, Carvajal-Castrillón A, Sierra-Pérez J. In-flight and wireless damage detection in a UAV composite wing using fiber optic sensors and strain field pattern recognition. *Mech. Syst. Signal Process.* 2020;136: 1-26.
10. Rufai O, Chandarana N, Gautam M, Potluri P, Gresil M. Cure monitoring and structural health monitoring of composites using micro-braided distributed optical fibre. *Compos. Struct.* 2020;254: 1-9.
11. Shipunov GS, Baranov MA, Nikiforov AS, Golovin D V., Tihonova AA. Study smart-layer effect on the physical and mechanical characteristics of the samples from polymer composite materials under quasi-static loading. *PNRPU Mech. Bull*. 2020;2020(4): 188-200.
12. Shipunov GS, Baranov MA, Nikiforov AS, Tikhonova AA, Osokin VM, Tret'yakov AA. Creation of a SMART Layer prototype with fiber-optic sensors for monitoring the stress–strain state of structures fabricated from polymeric composite materials and an estimation of its technical characteristics. *J. Opt. Technol.* 2021;88(4): 209-214.
13. Qing XP, Beard SJ, Kumar A, Chan HL, Ikegami R. Advances in the development of built-in diagnostic system for filament wound composite structures. *Compos. Sci. Technol.* 2006;66(11-12): 1694-1702.
14. Qing X, Kumar A, Zhang C, Gonzalez IF, Guo G, Chang FK. A hybrid piezoelectric/fiber optic diagnostic system for structural health monitoring. *Smart Mater. Struct.* 2005;14(3): 98-103.
15. Yoon HJ, Song KY, Choi C, Na HS, Kim JS. Real-Time Distributed Strain Monitoring of a Railway Bridge during Train Passage by Using a Distributed Optical Fiber Sensor Based on Brillouin Optical Correlation Domain Analysis. *J. Sensors.* 2016;2016: 1-10.
16. Scott RH, Banerji P, Chikermane S, Srinivasan S, Basheer PAM, Surre F et al. Commissioning and evaluation of a fiber-optic sensor system for bridge monitoring. *IEEE Sens. J.* 2013;13(7): 2555–2562.
17. Scott RH, Chikermane S, Vidakovic M, McKinley B, Sun T, Banerji P et al. Development of low cost packaged fibre optic sensors for use in reinforced concrete structures. *Meas. J. Int. Meas. Confed.* 2019;135: 617-624.
18. Prabhakar MM, Saravanan AK, Lenin AH, Leno IJ, Mayandi K, Ramalingam PS. A short review on 3D printing methods, process parameters and materials. *Mater. Today Proc.* 2020;45: 6108-6114.
19. Matveenko VP, Kosheleva NA, Serovaev GS, Fedorov AY. Numerical analysis of the strain values obtained by FBG embedded in a composite material using assumptions about uniaxial stress state of the optical fiber and capillary on the Bragg grating. *Frat. Ed. Integrita Strutt.* 2019;13(49): 177-89.
20. Voronkov AA, Anoshkin AN, Nikhamkin MA, Shipunov GS, Sazhenkov NA, Nikiforov AS. Registration of dynamic deformations of a composite material by fiber-optic sensors. *AIP Conf. Proc.* 2020;2216: 1-6.
21. Alemohammad H. Opto-Mechanical Modeling of Fiber Bragg Grating Sensors. In: *Opto-Mechanical Fiber Optic Sensors: Research, Technology, and Applications in Mechanical Sensing*. Canada: Elsevier; 2018. p.1–26.
22. Takeda S, Sato M, Ogasawara T. Simultaneous measurement of strain and temperature using a tilted fiber Bragg grating. *Sensors Actuators A Phys.* 2022;335: 113346.
23. Matveenko VP, Shardakov IN, Voronkov AA, Kosheleva NA, Lobanov DS, Serovaev GS, Spaskova EM, Shipunov GS. Measurement of strains by optical fiber Bragg grating

sensors embedded into polymer composite material. *Struct. Control Health Monit.* 2018;25(3): 1-11.

THE AUTHORS

Shipunov G.S.
e-mail: gsshipunov@gmail.com
ORCID: 0000-0002-2322-1872

Baranov M.A.
e-mail: maximbaranov.123@gmail.com
ORCID: 0000-0002-5600-1526

Nikiforov A.S.
e-mail: aleksandr.niciforov@gmail.com
ORCID: 0000-0001-5360-2484

Khabibrakhmanova F.R.
e-mail: faridhin@mail.ru
ORCID: 0000-0002-8078-6757